

# Self-Assembled Flexible Microlasers

Van Duong Ta, Rui Chen, and Han Dong Sun\*

Microlasers are in high demanded for many applications, such as photonic integrated circuits, quantum information processing, and the platform for investigation of light–matter interactions.<sup>[1–9]</sup> Up to date, fabrication of solid state microresonators has primarily been based on semiconductor materials, using either top-down or bottom-up techniques.<sup>[10]</sup> For the top-down approach, a microstructure can be obtained by etching an epitaxially grown planar cavity.<sup>[11]</sup> This approach critically relies on epitaxial growth, thus requiring costly apparatus and sophisticated growth techniques. Meanwhile, the strict requirement of lattice-matching between the epitaxial layers and the substrate severely limits material choices. Moreover, this method introduces optical losses at the boundary due to the imperfection of the etching, leading to low quality (*Q*) factors of the microresonators. In comparison, for the bottom-up approach, the microcavities are directly formed by self-assembled crystallization of nanostructures. This approach still calls for precise control of the shape, location, and size of the structures.<sup>[12–15]</sup> To solve this problem, soft microcavities such as microdroplets and liquid crystals have attracted increasing attention in recent years due to the simple fabrication and doping flexibility.<sup>[16,17]</sup>

For spherical microresonators such as microdroplets, the light is trapped due to total internal reflection at the interface.<sup>[16]</sup> Therefore, by embedding active materials into a microdroplet, optical emission can be selectively enhanced by the resonance known as whispering gallery modes (WGMs).<sup>[16–23]</sup> However, the instability of microdroplets and the complex trapping system largely hinder its practical application.<sup>[21,22]</sup> Obviously, a solid-state microresonator fabricated from soft matter but supported by a substrate is advantageous in terms of both stability and flexibility. Inspired by this motivation, microresonator made from organic polymers on a hydrophobic substrate was reported.<sup>[24]</sup> Unfortunately, there is no lasing observed from this structure, which might be due to the weak coupling of the emission into the WGM, high absorption of pumping wavelength by the polymer, or the poor quality of the cavity (low *Q* factor).

In this work, we report high-quality, self-assembled flexible microresonators, which demonstrate excellent WGM lasing upon optical pumping at room temperature. Flexible

hemispherical microresonators on distributed Bragg reflector (DBR) substrates are achieved using the hydrophobic effect. Both the size and position of the hemispheres can be tuned by this simple approach. The size tunability allows us to study the size-dependent optical characteristics of the structure. Laser emission from individual hemispheres is examined by a microphotoluminescence ( $\mu$ -PL) system, and the mechanism of lasing can be explained well by a 2D WGM model. Moreover, the mode spacing and *Q* factors of the microcavities are analyzed, and the relationship between the resonant energy of lasing spectrum and the mode numbers is discussed. Numerical simulations show a 3D confinement of emitted light inside the hemisphere, due to the high reflectivity of the DBR and total internal reflection at the interface between the hemisphere and the air, which verifies the existence of WGM microcavities.

The flexible hemispherical microresonators on DBR substrates are achieved as shown in **Figure 1**. Firstly, the DBR was deposited by electron beam evaporation on a glass substrate (**Figure 1d,e**). The DBR used herein consisted of 27 pairs of alternating SiO<sub>2</sub> and TiO<sub>2</sub> quarter-wave layers. The stop-band width of the DBR was about 140 nm, with a reflectivity of about 99.5% at 630 nm. A layer of 1H,1H,2H,2H-perfluorooctyltriethoxysilane (the hydrophobic layer) was then deposited over the topmost layer of the DBR by spin coating (**Figure 1f**). This layer increases the hydrophobic effect by surface modification.<sup>[24]</sup> In addition, the commercially available epoxy resin (Araldite 506 from Sigma-Aldrich) was chosen as a host material for the hemisphere due to its high viscosity, transparency, thermal stability against oxidation, and low-cost, which are suitable to form a high-quality and stable microresonator. To prepare the solution for the creation of hemispheres, the epoxy resin was dissolved in chloroform (CHCl<sub>3</sub>) with a volume ratio of 8:1. A high concentration of the epoxy resin was used in order to maintain a reasonable solution viscosity, which helps to prevent shrinkage of the hemispherical structures after solvent evaporation. The solution was then doped with 4 mM molecular Rhodamine 6G (R6G). The same hydrophobic layer was then coated onto a small cylindrical tip (**Figure 1a,b**) by a soft felt. It is noted that the cylindrical shape of the tip was chosen because it enables minimal contact with a planar surface. As shown in **Figure 1b**, a small amount of solution was spread on the tip. It was found that after several minutes, a line of discrete ‘droplets’ were spontaneously created and hung on the tip due to both gravitational and hydrophobic effects, as shown in **Figure 1c**. These ‘droplets’ were well aligned, which enabled us to achieve a line of hemispheres on the DBR later. Finally, the tip with the ‘droplets’ was carefully lowered to the DBR surface (**Figure 1g**) and then moved away after gentle contact (**Figure 1h**). As a result, a line of hemispherical microresonators were transferred onto the DBR surface from the tip. It is interesting to note that the

V. D. Ta,<sup>[\*]</sup> Dr. R. Chen,<sup>[\*]</sup> Prof. H. D. Sun  
Division of Physics and Applied Physics  
School of Physical and Mathematical Sciences  
Nanyang Technological University  
Singapore 637371, Singapore  
E-mail: hdsun@ntu.edu.sg



[\*] These authors contributed equally to this work.

DOI: 10.1002/adma.201103409

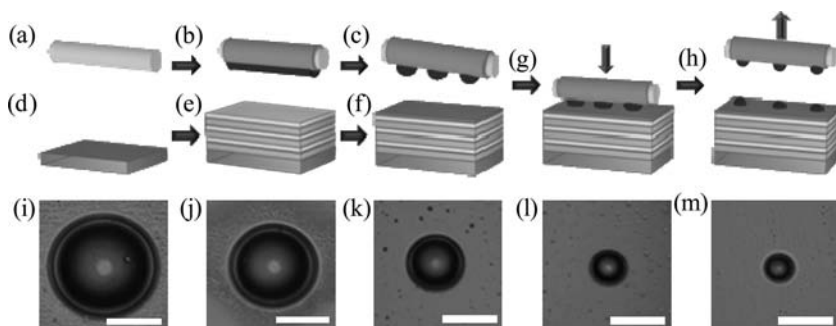


**Figure 1.** a–c) Creation of ‘droplets’ on a cylindrical tip. d–f) Deposition of the DBR and hydrophobic layer. g) The ‘droplets’ are transferred from the tip onto the DBR surface. h) The hemispheres are formed on the DBR surface. i–m) Top-down view optical images of hemispherical resonators with different sizes under halogen illumination. The scale bars are 50  $\mu\text{m}$ .

tip can be reused for creating smaller hemispheres by subsequent depositions. By doing so, the size of the hemispheres can be changed from large ( $\approx 120 \mu\text{m}$ ) to small ( $\approx 5 \mu\text{m}$ ), maintaining perfect circular structures. In addition, the number of hemispheres created can be modified by the length of active solution, as shown in Figure 1b. Therefore, we can obtain a single hemisphere if the length is short enough. These structures were dried in air for 24 h and then in an oven at  $80 \text{ }^\circ\text{C}$  for 1 h. This treatment helps to evaporate the solvent fully and stabilize the hemispheres. Figure 1i–m display the optical image of our hemispherical structures with diameters from about 100 to 25  $\mu\text{m}$ .

Optical measurement of the created structure was carried out (see Experimental Section for details). **Figure 2** depicts the  $\mu\text{-PL}$  spectra (Figure 2a) from a single hemisphere (images attached in Figure 2b, showing a diameter of about 80  $\mu\text{m}$ ) at room temperature. It can be seen that the PL intensity increases with increasing pump pulse energy (PPE) of the incident laser, and lasing emission was observed under PPE = 2.8  $\mu\text{J}$ . In order to examine the lasing action, a few of the PL spectra around this threshold are enlarged in the inset of Figure 2a, which shows clearly the trend from spontaneous emission with a broadened spectrum (PPE = 0.5–1.8  $\mu\text{J}$ ) to lasing emission with sharp peaks. Analysis of lasing peaks under higher PPE will be discussed later. In addition, an integrated PL intensity of the peaks with PPE is shown in Figure 2b. A nonlinear increase of the emission intensity supports the lasing action, and the lasing threshold was found to be around 2.6  $\mu\text{J}$ .

We tentatively analyzed the lasing mechanism based on a 2D WGM model, supposing

the radial mode number  $r = 1$ .<sup>[24]</sup> Under this assumption, the resonant wavelength of the WGM can be calculated from following equation,

$$m = \pi Dn/\lambda_m \quad (1)$$

where  $m$  is the angular mode number and  $D$  and  $n$  are the diameter and effective refractive index of the hemisphere, respectively.<sup>[24]</sup> The value of  $m$  can be estimated as  $m = \lambda_{m+1}/(\lambda_m - \lambda_{m+1})$ , with  $\lambda_{m+1}$ ,  $\lambda_m$  being the resonance wavelengths for mode numbers  $m+1$  and  $m$ , respectively.  $D$  can be estimated from the optical image, which then allows us to calculate  $n$ . The calculated  $n$  is 1.41 assuming  $D = 80.14 \mu\text{m}$ , and the corresponding

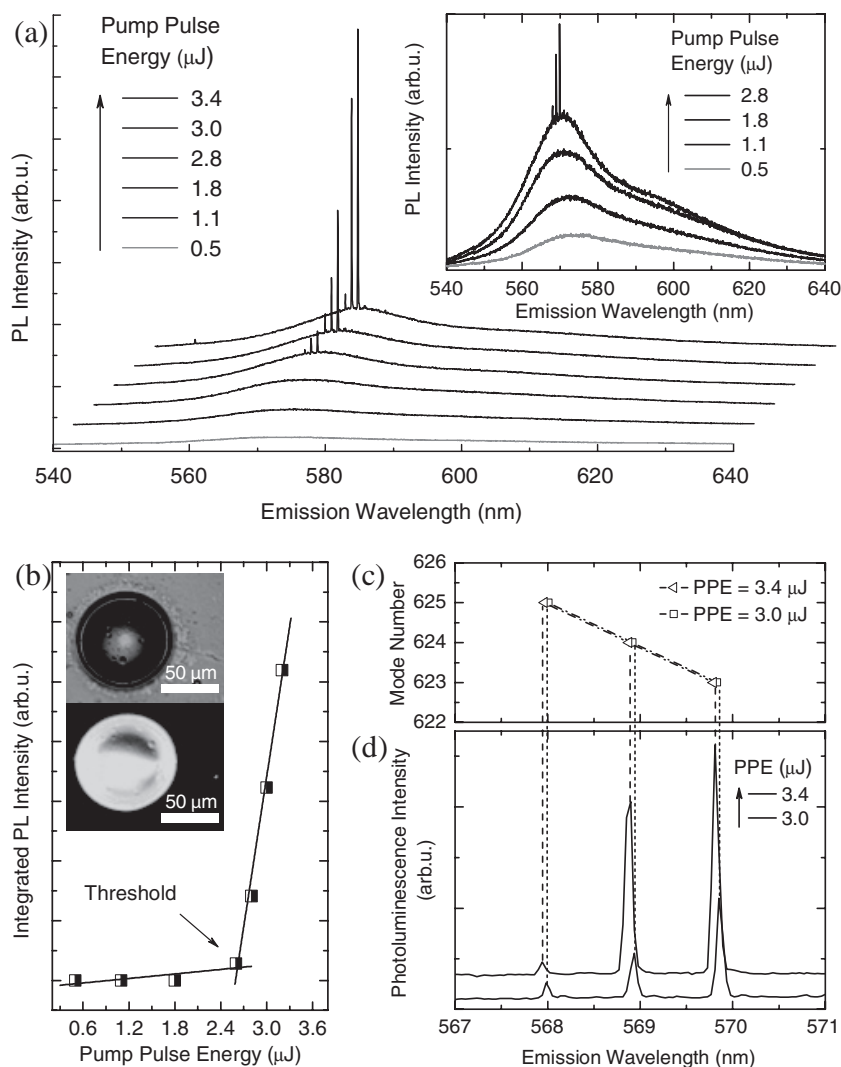


**Figure 2.** a) The PL emission recorded at room temperature as a function of pump pulse energy. The inset enlarges the part of the  $\mu\text{-PL}$  spectrum in the low range of excitation density. b) The integrated PL intensity dependence on the excitation power. The optical image (top) and PL image (bottom) of the hemisphere are given in the inset. c) Calculation of WGM lasing mode numbers. d) The corresponding lasing spectrum.

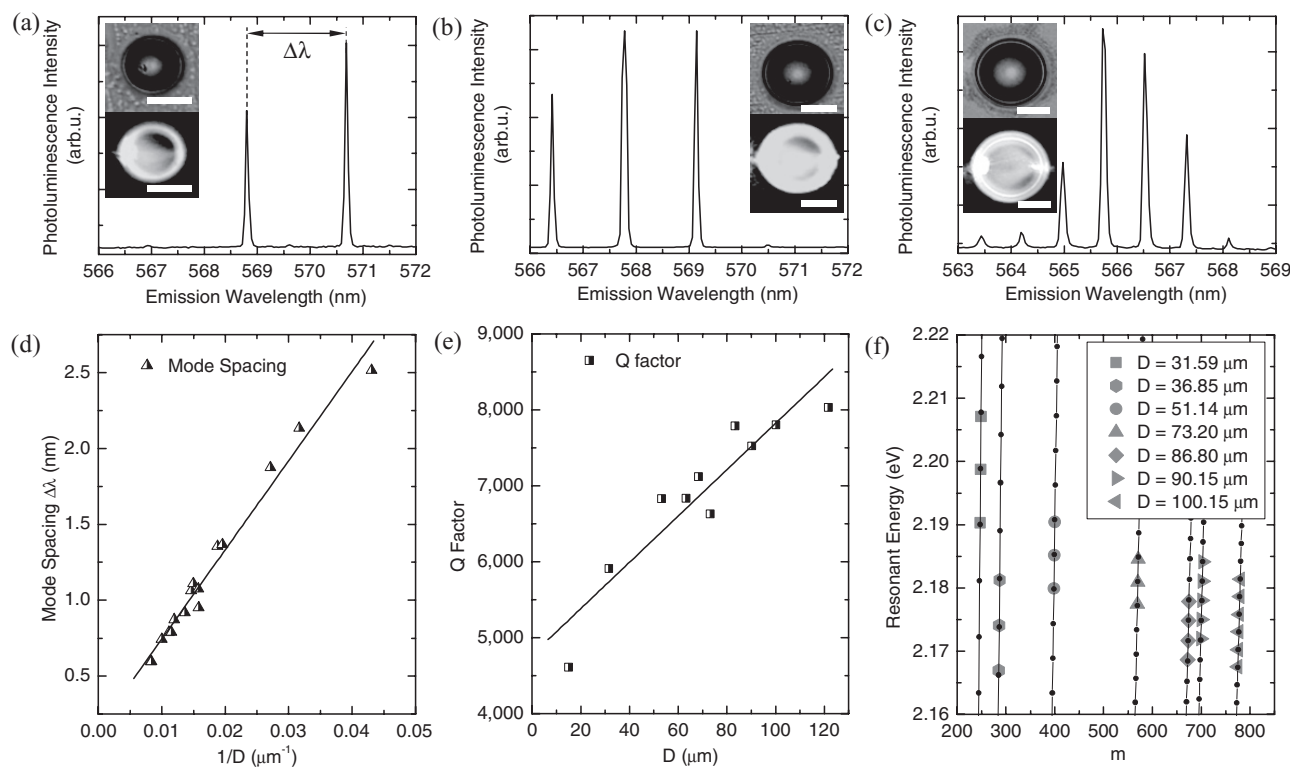


**Figure 3.** a–c) The  $\mu$ -PL spectrum of hemispheres with different diameters. The insets show optical and PL images of the hemispheres. d,e) The mode spacing and  $Q$  factors as a function of reciprocal diameter and diameter of the hemispheres. f) Lasing photon energy (large symbols) compared with theoretical data. The solid dots indicate predicted values, determined from Equation (1). The scale bars are 50  $\mu\text{m}$ .

mode numbers are indexed as 623–625 (Figure 2c). We found that these values match well with the lasing peaks presented in Figure 2d, which supports the WGM lasing mechanism. Moreover, as can be seen from Figure 2d, the lasing peaks show a little blueshift under higher PPE. The reason for this phenomenon can be ascribed to a slight change of the hemisphere's refractive index due to a thermal effect generated by pumping.<sup>[25]</sup>

The characteristics of the WGM lasing action were further investigated by examining the mode spacing, as well as  $Q$  factors of hemispheres with different sizes. Mode spacing provides information about cavity length ( $\Delta\lambda \sim 1/D$ ), while the  $Q$  factor is an important qualitative parameter of a laser cavity.<sup>[12]</sup> The mode spacing ( $\Delta\lambda$ ) is shown in Figure 3a, gradually decreasing with increasing hemisphere size (Figure 3a–c). It is found that the experimentally measured mode spacing is proportional to the reciprocal diameter of a hemisphere (Figure 3d).<sup>[26]</sup> Moreover, the  $Q$  factor (defined as  $Q = \lambda/\delta\lambda$ , where  $\lambda$  is the peak wavelength and  $\delta\lambda$  is the line-width of the peak, respectively) exhibits linear dependence on hemispherical diameters (Figure 3e). This is reasonable because increasing the hemispherical diameter means increasing both cavity length ( $L$ ), and reflectivity ( $R$ ) at the hemisphere–air interface. These two factors push the  $Q$  factor up based on following equation  $Q = 2\pi nL/\lambda(1-R)$ .<sup>[13]</sup> It can be seen from Figure 3e that the  $Q$  is around 4500 for  $D = 15 \mu\text{m}$ , increasing to approximately 8000 for  $D = 122 \mu\text{m}$ . This value is higher than those of the microcavities reported in spherical microdroplets<sup>[17]</sup> and micropillars.<sup>[11]</sup>

In order to get a clearer picture of the mode spacing dependence on the hemispherical diameter, the resonant energy of WGM cavities as a function of mode number is presented in Figure 3f.<sup>[14]</sup> The mode spacing is the spatial distance between lasing peaks (big symbols), which regularly decreases with increasing  $m$ , corresponding to the increase of hemispherical size. The experimental observations fit well with theoretical predictions (line–symbols), which implies that the lasing mechanism from the hemisphere is indeed ascribed to 2D WGM.

The DBR is supposed to play an indispensable role in achieving lasing in these experiments, as it helps to confine the emission inside the hemisphere in the vertical direction. Moreover, light is trapped in the horizontal direction due to total internal reflection at the hemisphere–air interface. As a result, all emission from the dye will be three-dimensionally confined inside the cavity and form WGM. Using the finite element method supported by COMSOL Multiphysics, numerical simulations were performed to determine the field distribution in the structure.<sup>[27]</sup> The refractive index of the substrate is approximately 1.54.<sup>[28]</sup> The calculated field distribution inside the hemispherical microcavities is shown in Figure 4b–c. The resonant modes of WGM in the circumference are demonstrated in Figure 4b, where the total reflection can be seen at the hemisphere–air interface. The mode profile of WGM in the vertical direction indicates a single resonant peak corresponding to a single cavity, as shown in Figure 4c. Consequently, the light can be considered to travel in a circular cavity, as schematically drawn in Figure 4a. This simulated result supports the

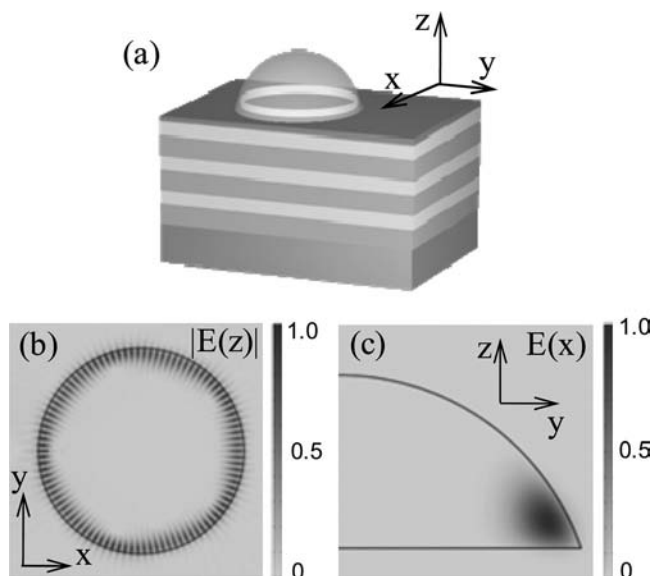


**Figure 4.** a) The 3D schematic of a hemisphere. The white circle inside the hemisphere indicates the WGM loop. b) Absolute electric field inside a hemisphere in the horizontal plane. c) Electric field profile of the WGM in a hemisphere in the vertical plane.

WGM cavity and provides a picture of a real cavity inside the hemisphere.

As a control experiment, we replaced the DBR with a simple glass substrate. In this situation, there was no lasing observed from hemispheres under the same experimental conditions. As it is well known, the emission from dye molecules inside a hemisphere is emitted uniformly in all directions. However, due to the higher refractive index of the substrate (1.54) compared to the hemisphere, the emitted light prefers to penetrate the substrate. As a result, there is no confinement in the vertical direction. For the horizontal plane, a WGM still can be formed due to the total internal reflection. However, this confinement is only in 2D and, thus, the lasing threshold should be much higher as compared to the previous case. This could explain why there is no lasing observed from the sample without the bottom DBR.

In conclusion, we have reported a simple method for fabricating truly 3D-confined hemispherical microresonators with tunable size and position. The proposed approach does not require sophisticated microfabrication techniques. WGM lasing emission with a very high  $Q$  factor from dye-doped hemispheres was observed at room temperature. Size-dependent lasing characteristics have been investigated, showing an agreement between experimental observation and theoretical calculation. It is important to note that numerous active materials such as colloidal quantum dots or semiconductor nanowires can be easily incorporated into the cavity by a similar approach, which points out the doping flexibility of our proposed structure. Owing to the fabrication simplicity, arrays of microcavities and coupled cavities can be readily produced, which may allow their use in novel photonic device applications such as high-precision optical filters, or for optical bistability and quantum information processing. The proposed structure also provides

an excellent platform for fundamental studies of, for example, cavity quantum electrodynamics in the strong coupling regime and nonlinear optical phenomena.

## Experimental Section

Optical characteristics of individual hemispheres were studied using the  $\mu$ -PL system. The excitation source was a frequency-doubled, Q-switched Nd:YAG laser which generates green emission at 532 nm with a pulse width of 1 ns and a frequency of 60 Hz. The laser was guided at an angle of about  $45^\circ$  to normal of the sample and focused to a beam spot size with a diameter of 1.5 mm to pump the hemisphere. Emission spectra were collected by an objective (50 $\times$ , numerical aperture = 0.42), and delivered to a camera for a PL image or to silicon charge-coupled device (CCD) for recording spectra with a spectral resolution of 0.05 nm. In addition, to avoid oxidation of the molecular dyes, the hemisphere was pumped only in discrete periods of 200 ms during a spectral scanning process of the CCD.

## Acknowledgements

Support from the Singapore Ministry of Education through the Academic Research Fund (Tier 1) under Project No. RG63/10 and from the Singapore National Research Foundation through the Competitive Research Programme (CRP) under Project No. NRF-CRP6-2010-02 is gratefully acknowledged.

Received: September 4, 2011

Revised: November 17, 2011

Published online: February 10, 2012

- [1] O. Painter, R. K. Lee, A. Scherer, A. Yariv, J. D. O'Brien, P. D. Dapkus, I. Kim, *Science* **1999**, *284*, 1819.
- [2] S. Noda, A. Chutinan, M. Imada, *Nature* **2000**, *407*, 608.
- [3] K. J. Vahala, *Nature* **2003**, *424*, 839.
- [4] Y. Akahane, T. Asano, B. S. Song, S. Noda, *Nature* **2003**, *425*, 944.
- [5] S. Noda, *Science* **2006**, *314*, 260.
- [6] S. Strauf, K. Hennessy, M. T. Rakher, Y. S. Choi, A. Badolato, L. C. Andreani, E. L. Hu, P. M. Petroff, D. Bouwmeester, *Phys. Rev. Lett.* **2006**, *96*, 127404.
- [7] R. Kirchain, L. Kimerling, *Nat. Photonics* **2007**, *1*, 303.
- [8] M. Humar, I. Musevic, *Opt. Express* **2010**, *18*, 26995.
- [9] H. C. Yi, K. W. Yi, L. J. Guo, *Appl. Phys. Lett.* **2011**, *98*, 131109.
- [10] C. Z. Ning, *Phys. Stat. Solidi B* **2010**, *247*, 774.
- [11] R. Chen, H. D. Sun, T. Wang, K. N. Hui, H. W. Choi, *Appl. Phys. Lett.* **2010**, *96*, 241101.
- [12] A. C. Tamboli, E. D. Haberer, SharmaRajat, K. H. Lee, S. Nakamura, E. L. Hu, *Nat. Photonics* **2007**, *1*, 61.
- [13] R. Chen, B. Ling, X. W. Sun, H. D. Sun, *Adv. Mater.* **2011**, *23*, 2199.
- [14] C. Czekalla, T. Nobis, A. Rahm, B. Cao, J. Zúñiga-Pérez, C. Sturm, R. Schmidt-Grund, M. Lorenz, M. Grundmann, *Phys. Stat. Solidi B* **2010**, *247*, 1282.
- [15] D. J. Gargas, M. C. Moore, A. Ni, S.-W. Chang, Z. Zhang, S.-L. Chuang, P. Yang, *ACS Nano* **2010**, *4*, 3270.
- [16] M. Humar, M. Ravnik, S. Pajk, I. Musevic, *Nat. Photonics* **2009**, *3*, 595.
- [17] S. K. Y. Tang, R. Derda, Q. Quan, M. Loncar, G. M. Whitesides, *Opt. Express* **2011**, *19*, 2204.
- [18] H. B. Lin, A. L. Huston, B. L. Justus, A. J. Campillo, *Opt. Lett.* **1986**, *11*, 614.

- [19] S. X. Qian, J. B. Snow, H. M. Tzeng, R. K. Chang, *Science* **1986**, 231, 486.
- [20] M. M. Mazumder, G. Chen, P. J. Kindlmann, R. K. Chang, J. B. Gillespie, *Opt. Lett.* **1995**, 20, 1668.
- [21] A. Kiraz, M. A. Dunder, A. L. Demirel, S. Doganay, A. Kurt, A. Sennaroglu, M. Y. Yuce, *J. Nanophoton.* **2007**, 1, 011655.
- [22] J. Schäfer, J. P. Mondia, R. Sharma, Z. H. Lu, A. S. Sussha, A. L. Rogach, L. J. Wang, *Nano Lett.* **2008**, 8, 1709.
- [23] S. K. Y. Tang, Z. Y. Li, A. R. Abate, J. J. Agresti, D. A. Weitz, D. Psaltis, G. M. Whitesides, *Lab Chip* **2009**, 9, 2767.
- [24] J. Haase, S. Shinohara, P. Mundra, G. Risse, V. G. Lyssenko, H. Frob, M. Hentschel, A. Eychmuller, K. Leo, *Appl. Phys. Lett.* **2010**, 97, 211101.
- [25] H. J. Moon, Y.-T. Chough, J. B. Kim, K. An, J. Yi, J. Lee, *Appl. Phys. Lett.* **2000**, 76, 3679.
- [26] H. Taniguchi, J. Kido, M. Nishiya, S. Sasaki, *Appl. Phys. Lett.* **1995**, 67, 1060.
- [27] M. Oxborrow, *IEEE Trans. Microw. Theory Tech.* **2007**, 55, 1209.
- [28] G. Ghosh, *Opt. Commun.* **1999**, 163, 95.
-